JOURNAL OF MATERIALS SCIENCE 30 (1995) 219–224

A modified analysis for stress transfer in fibre-reinforced composites with bonded fibre ends

CHUN-HWAY HSUEH
Metals and Ceramics Division, Oak Ridge National Laboratory Oak Ridge, Tennessee 37831, USA

The elastic stress transfer from the matrix to the embedded fibre in fibre-reinforced composites has been analysed previously when the loading direction is parallel to the fibre axis and the fibre is bonded to the matrix. Stress transfer occurs both at the interface along the fibre length and at the ends of the fibre. However, the boundary condition at the bonded ends is ambiguous, and various assumptions have been made to obtain solutions for this stress transfer problem. To satisfy more rigorously the boundary condition for the bonded ends, a new technique of assuming imaginary fibres in the composite is proposed in the present study. Compared to the previous analytical solution, the present analytical solution bears more physical meaning and is in better agreement with numerical and experimental results

1. Introduction

Substantial reinforcement can be achieved by incorporating aligned fibres in a matrix with the fibre axis parallel to the loading direction [1, 2]. The mechanics of reinforcement relies on stress transfer from the matrix to the embedded fibres during loading. To analyse this stress transfer, the shear lag model [3–14] has been used extensively in which a representative volume element containing one fibre (see Fig. 1 below) is adopted for analysis.

In the classical shear lag model [3], the ends of the embedded fibre are assumed to debond from the matrix and stress transfer occurs only at the interface along the fibre length. At these debonded ends, the stress is free and the boundary condition in solving the stress transfer problem is trivial. When the ends of the fibre are bonded to the matrix, stress transfer also occurs at the bonded ends, and the stress at the bonded ends is finite. However, this finite stress is not a predetermined value, and the boundary condition at the bonded ends becomes ambiguous. Different assumptions have been made to analyse the stress transfer problem with bonded fibre ends. In the solutions obtained by polynomial approximation [15], a constant axial stress or displacement is assumed in the matrix at the cross-section corresponding to the fibre ends. In the solutions obtained by the finite element method [16], a uniform axial displacement is adopted at the end of the matrix. In the finite difference analysis [17], the lattice in the composite is strained by a constant amount; then, a technique of over-relaxation or block relaxation is used to calculate the displacement in the equilibrium condition. In the previous analytical solution [12] it was assumed that at the least perturbed positions (due to the presence of the fibre) the axial stress is equal to the applied stress.

As a complement to the previous study [12], the purpose of the present study is to adopt a more rigorous boundary condition for the bonded ends to obtain analytical solutions for the stress transfer problem. First, the previous analytical solution [12] is summarized. Second, a new technique of adding imaginary fibres in the shear lag model is developed to define a more rigorous boundary condition for the bonded ends and to obtain a more meaningful analytical solution. Third, the present analytical solution is compared with the previous analytical solution [12] and the existing numerical solution [17]. Finally, effects of the distance between the bonded ends and the loading surface, the aspect ratio of the fibre, and the Young's modulus ratio of fibre to matrix on stress transfer are shown. A critical fibre length for effective stress transfer [18] is also defined and compared with the experimental measurements [19].

2. Summary of the previous analytical solution

The shear lag model is shown in Fig. 1. A fibre with radius a and length $2l$ is embedded at the centre of a coaxial cylindrical matrix with a radius b and length $2l'$. The cylindrical coordinates r, θ and z are used. A tensile stress σ_0 is applied to the composite in the z direction. The fibre is bonded to the matrix at both the interface (i.e. at $r = a$) and the ends ($z = \pm l$). The stress is transferred from the matrix to the fibre through both the interface and the fibre ends.

The general solutions for the axial stress distribution in the fibre, σ_f, and the interfacial shear stress, τ_a, along the fibre length for the problem depicted in Fig. 1 have been derived, such that [12]

0022–2461 © *1995 Chapman & Hall*

$$\sigma_f = \frac{b^2 E_f \sigma_0}{a^2 E_f + (b^2 - a^2) E_m} + A \exp(\alpha z) + B \exp(-\alpha z) \quad (1)$$

$$\tau_a = -\frac{a\alpha}{2} [A \exp(\alpha z) - B \exp(-\alpha z)] \quad (2)$$

where

$$\alpha = \frac{1}{a} \left(\frac{a^2 E_f + (b^2 - a^2) E_m}{(1 + \nu_m) E_f [b^2 \ln(b/a) - (b^2 - a^2)/2]} \right)^{1/2} \quad (3)$$

E and ν are Young's modulus and Poisson's ratio, and the subscripts f and m denote the fibre and the matrix, respectively. Determination of the coefficients A and B is contingent upon the boundary condition at the ends of the fibre.

The stress at the bonded ends is finite. However, this finite stress is not a predetermined value which, in turn, results in difficulties in determining A and B. In the previous analysis [12], instead of defining an exact boundary condition for the bonded ends, an alternative boundary condition in an approximate manner is adopted. It is noted that within the region $-l \leq z \leq l$ and $r \leq b$, the least perturbed positions (due to the presence of the fibre) are located at $z = \pm l$ and $r = b$. Hence, axial stresses at these positions are assumed to be unperturbed and equal to the applied stress, such that

$$\sigma_m = \sigma_0 \quad \text{at} \quad z = \pm l, \quad r = b \quad (4)$$

The solution for A and B based on the above assumption (Equation 4) are [12]

$$A = \frac{a^2 (E_m - E_f) \sigma_0}{a^2 E_f + (b^2 - a^2) E_m} \left(\frac{b^2 - a^2}{2 \ln(b/a)} - b^2 \right) \left\{ \left[\left(a^2 - \frac{b^2 - a^2}{2 \ln(b/a)} \right) \frac{E_m}{E_f} - a^2 \right] [\exp(\alpha l) + \exp(-\alpha l)] \right\}^{-1} \quad (5a)$$

$$B = A \quad (5b)$$

3. The present analytical solution

The boundary condition at the bonded ends is defined by the continuity condition at $z = \pm l$. To satisfy this continuity condition, a news technique of adding imaginary fibres to the shear lag model is developed. The matrix above and below the fibre (see the area between dashed lines in Fig. 1) is treated as two imaginary fibres which have the matrix properties. The geometry in Fig. 1 is symmetric, and only the region $z \geq 0$ is considered. The physical meaning of the analytical procedures need in solving this problem is stated as follows. A uniform stress σ_0 is loaded on the imaginary fibre and the matrix at $z = l'$. The stress is transferred between the imaginary fibre and the matrix in the region $l \leq z \leq l'$. At $z = l$ the stress is continuous between the imaginary fibre and the real fibre. The stress thus transfers between the real fibre and the matrix in the region $0 \leq z \leq l$.

Whereas the general solutions for σ_f and τ_a in the real fibre are described by Equations 1 and 2, the general solutions for the stress distribution σ_f' and the interfacial shear stress τ_a' in the imaginary fibre can be obtained by replacing E_f with E_m in Equations 1 to 3, such that

$$\sigma_f' = \sigma_0 + A' \exp(\alpha' z) + B' \exp(-\alpha' z) \quad l \leq z \leq l' \quad (6)$$

$$\tau_a' = \frac{-a\alpha'}{2} [A' \exp(\alpha' z) - B' \exp(-\alpha' z)] \quad l \leq z \leq l' \quad (7)$$

where

$$\alpha' = \frac{b}{a} \left\{ (1 + \nu_m) \left[b^2 \ln\left(\frac{b}{a}\right) - \frac{b^2 - a^2}{2} \right] \right\}^{-1/2} \quad (8)$$

To obtain the coefficients A and B for the real fibre and A' and B' for the imaginary fibre, four boundary conditions are required which are

$$\sigma_f' = \sigma_0 \quad \text{at} \quad z = l' \quad (9a)$$

$$\sigma_f = \sigma_f' \quad \text{at} \quad z = l \quad (9b)$$

$$\tau_a = \tau_a' \quad \text{at} \quad z = l \quad (9c)$$

$$\tau_a = 0 \quad \text{at} \quad z = 0 \quad (9d)$$

Equation 9a is the loading condition, Equations 9b and c are the continuity conditions, and Equation 9d is the symmetry condition.

The solutions for A, B, A' and B' subjected to the above boundary conditions are

$$A = \frac{(b^2 - a^2)(E_m - E_f)\sigma_0}{a^2 E_f + (b^2 - a^2) E_m} \left(\exp(\alpha l) + \exp(-\alpha l) - \frac{\alpha [\exp(\alpha l) - \exp(-\alpha l)][\exp(\alpha' l) - \exp\{\alpha'(2l' - l)\}]}{\alpha' [\exp(\alpha' l) + \exp\{\alpha'(2l' - l)\}]} \right)^{-1} \quad (10a)$$

$$B = A \quad (10b)$$

$$A' = \frac{\alpha [\exp(\alpha l) - \exp(-\alpha l)] A}{\alpha' \{\exp(\alpha' l) + \exp[\alpha'(2l' - l)]\}} \quad (10c)$$

$$B' = -A' \exp(2\alpha' l') \quad (10d)$$

Furthermore, when the bonded end is sufficiently remote from the loading surface such that $\exp(2\alpha' l') \gg \exp(\alpha' l)$, the coefficient A ($= B$) becomes

$$A = \frac{(b^2 - a^2)(E_m - E_f)\sigma_0}{a^2 E_f + (b^2 - a^2) E_m} \left(\frac{\alpha'}{\alpha' [\exp(\alpha l) + \exp(-\alpha l)] + \alpha [\exp(\alpha l) - \exp(-\alpha l)]} \right) \quad (11)$$

Also, under this condition the axial stress and the interfacial shear stress at the bonded ends have asymptotic values, such that

$$\sigma_f = \frac{\sigma_0}{a^2 E_f + (b^2 - a^2) E_m}\left(b^2 E_f + \frac{(b^2 - a^2)(E_m - E_f)\alpha'[\exp(\alpha l) + \exp(-\alpha l)]}{\alpha'[\exp(\alpha l) + \exp(-\alpha l)] + \alpha[\exp(\alpha l) - \exp(-\alpha l)]}\right) \quad \text{at } z = l \quad (12)$$

$$\tau_a = \frac{-a\alpha}{2}\left(\frac{(b^2 - a^2)(E_m - E_f)\sigma_0}{a^2 E_f + (b^2 - a^2) E_m}\right)\left(\frac{\alpha'[\exp(\alpha l) - \exp(-\alpha l)]}{\alpha'[\exp(\alpha l) + \exp(-\alpha l)] + \alpha[\exp(\alpha l) - \exp(-\alpha l)]}\right) \quad \text{at } z = l \quad (13)$$

4. Results

The present analytical solution is compared with some of the existing solutions. The stress transfer problem described in Fig. 1 has been analysed numerically by using a finite difference method [17]. However, to simplify the analysis, cubic lattices were adopted for both the fibre and the matrix in the finite difference analysis. Hence, instead of the cylindrical geometry depicted by Fig. 1, the geometry considered in the finite difference analysis is a rectangular parallelepiped [17]. This difference in geometry would result in differences in the magnitude of the calculated results; however, the trends obtained for both geometry should remain the same. The results were calculated using $b/a = 11$, $l/a = 50$, $l'/a = 100$, $\nu_f = \nu_m = 0.35$, and different values of E_f/E_m in the finite difference analysis [17]. Unless noted otherwise, the same material properties are adopted in the present calculation. First, a comparison is made between the present solution, the previous analytical solutions [12] and the finite difference solution [17]. Second, the effects of the distance between the fibre end and the loading surface (i.e. $l' - l$) are examined. Third, the effects of fibre length on stress transfer are shown, and a critical fibre

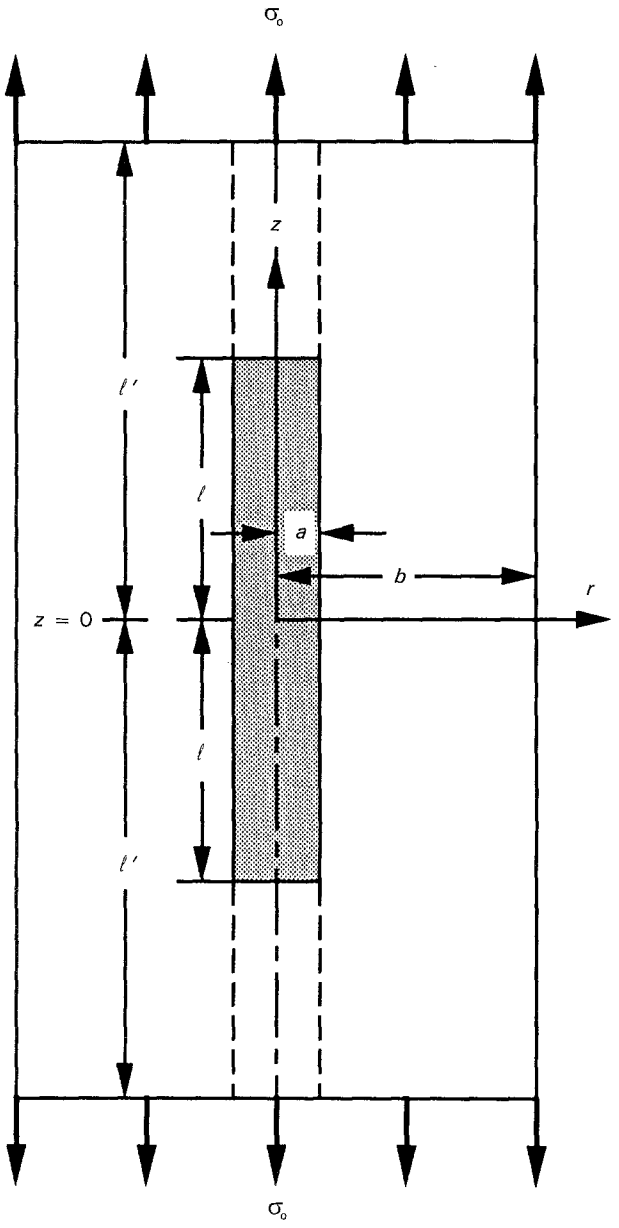

Figure 1 Schematic diagram showing the shear lag model for stress transfer from the matrix to the embedded fibre. Imaginary fibres (shown dashed) are added to analyse the case where the ends of the real fibre are bonded to the matrix.

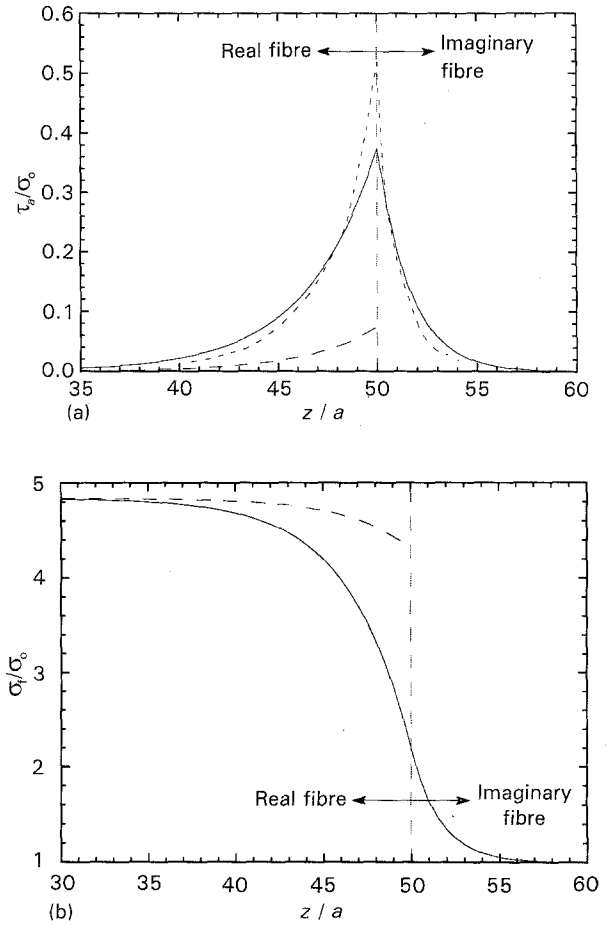

Figure 2 Comparison of distributions with normalized axial position, z/a, of (a) the normalized interfacial shear stress, τ_a/σ_0 (and τ'_a/σ_0), and (b) the normalized axial stress, σ_f/σ_0 (and σ'_f/σ_0), for (———) the present and (– –) the previous analytical solution and (- - -) the finite difference solution.

length for effective stress transfer is defined to compare with the experimental measurements [19]. Finally, the effects of the Young's modulus ratio E_f/E_m on stress transfer are studied. The axial stress and the interfacial shear stress are even and odd functions of z, respectively. Plots of the stress distribution along the z direction are shown only for $z \geq 0$ in this paper.

4.1. Comparison

The normalized interfacial shear stress and the normalized axial stress in the fibre as functions of the normalized axial position are shown, respectively, in Fig. 2a and b for $E_f/E_m = 5$. The boundary between the imaginary and the real fibres is also shown. The results obtained from the previous analytical solutions are limited to the region of $0 \leq z \leq l$ (i.e. the real fibre) [12], and results for the axial stress distribution are not available in the finite difference solution [17]. Fig. 2a shows that the maximum interfacial shear stress occurs at the end of the fibre (i.e. at $z = l$). Compared with the previous analytical results [12], the present analytical results are in better agreement with the numerical results (Fig. 2a). By assuming the least perturbed positions in the previous analytical solution [12], the maximum interfacial shear stress at the fibre ends is underestimated (Fig. 2a) and the finite axial stress at the bonded fibre ends is overestimated (Fig. 2b).

4.2. Effects of $l' - l$ on stress transfer

The distributions of the axial stress and the interfacial shear stress along the loading direction are shown in Fig. 3a and b, respectively, for $E_f/E_m = 5$ and different values of l'/a. The following results can be concluded from Fig. 3a. First, the loading stress on the imaginary fibre is σ_0, i.e. $\sigma_f' = \sigma_0$ at $z = l'$. The stress transfers from the matrix to the imaginary fibre because of the existence of the real fibre underneath. Second, at the boundary between the imaginary and the real fibres (i.e. at the end of the fibre, $z = l$), the axial stress has a finite value (Fig. 3a). This finite value increases with an increase in l', and reaches an asymptote dictated by Equation 12 when the loading surface is sufficiently remote from the end of the fibre. Third, the stress is continuously transferred from the matrix to the real fibre. The maximum axial stress in the real fibre reaches an equilibrium value when the fibre is sufficiently long; this will be discussed in section 4.3 below.

The maximum interfacial shear stress occurs at the end of the real fibre where discontinuities of material properties exist (Fig. 3b). In the absence of the real fibre, there is no stress transfer between the matrix and the imaginary fibre and the interfacial shear stress along the imaginary fibre is zero. When the end of the real fibre is closer to the loading surface (i.e. when l' decreases), the sense of material discontinuity by loading is stronger which in turn, results in an increase in interfacial shear stress.

It is noted that when the loading surface is sufficiently remote from the end of the real fibre, both σ_f and τ_a approach their asymptotic values (see Equations 12 and 13) at $z = l$. This condition is satisfied

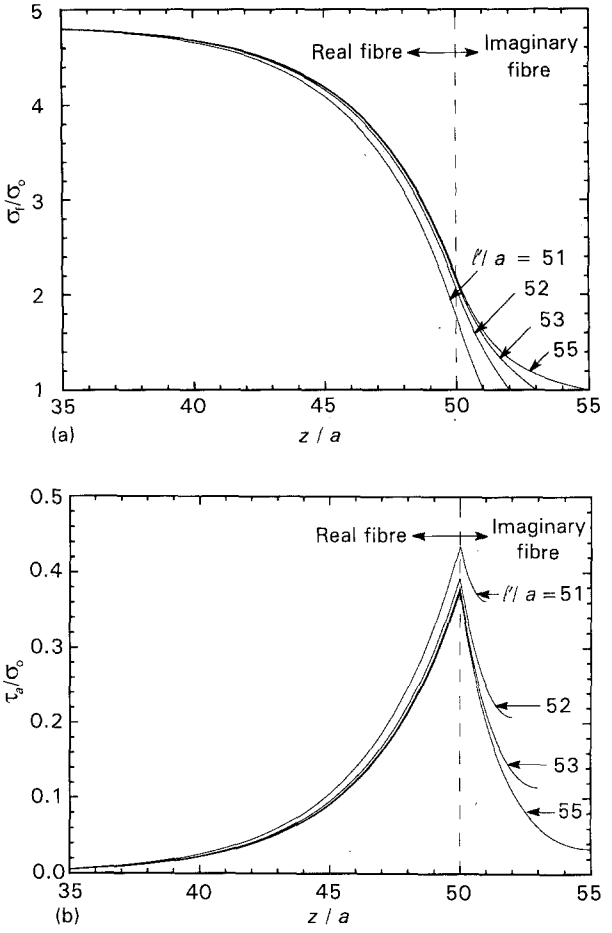

Figure 3 (a) Normalized axial stress, σ_f/σ_0 (and σ_f'/σ_0), and (b) normalized interfacial shear stress, τ_a/σ_0 (and τ_a'/σ_0), as functions of normalized axial position, z/a, at different values of l'/a.

when the loading surface is only about three times the fibre radius from the fibre end, i.e. when $(l' - l)/a \geq 3$ (see Fig. 3a and b). Hence, the loading surface is assumed to be sufficiently remote from the fibre end, and the effect of l' on stress transfer is ignored in the next section, which examines the effects of the aspect ratio of the fibre on stress transfer.

4.3. Effects of the aspect ratio

The effect of the aspect ratio of the fibre, l/a, on stress transfer is shown in Fig. 4. When the fibre is sufficiently long (e.g. $l/a \geq 30$), the maximum axial stress in the fibre reaches an equilibrium value such that

$$\sigma_f = \frac{b^2 E_f \sigma_0}{a^2 E_f + (b^2 - a^2) E_m} \quad \text{for } l \to \infty \qquad (14)$$

At this equilibrium state there is no stress transfer between the fibre and the matrix, the interfacial shear stress is zero, and both the fibre and the matrix have the same equilibrium axial strain ε_0, such that

$$\varepsilon_0 = \frac{b^2 \sigma_0}{a^2 E_f + (b^2 - a^2) E_m} \qquad (15)$$

A critical fibre length l_c has been defined [17, 18] such that at this critical length, the maximum fibre stress (i.e. the fibre stress at $z = 0$) equals 97% of that for an infinitely long fibre (i.e. Equation 14). The normalized

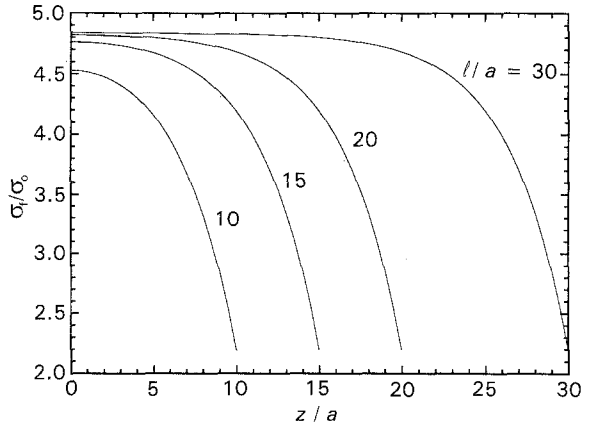

Figure 4 Normalized axial stress, σ_f/σ_0, as a function of normalized axial position, z/a, at different values of l/a.

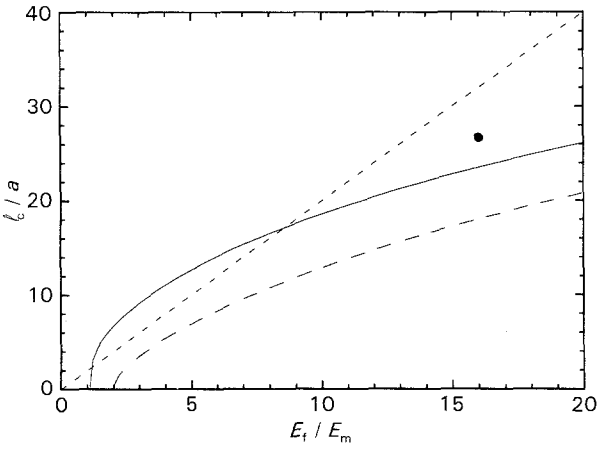

Figure 5 Normalized critical fibre length, l_c/a, for effective stress transfer as a function of the Young's modulus ratio, E_f/E_m: (——) present and (– –) previous analytical solution, (---) finite difference solution, (●) experimental.

critical fibre length as a function of the Young's modulus ratio, E_f/E_m, is shown in Fig. 5. The results obtained from the previous analytical solution [12], the finite difference solution [17] and the experimental measurements of polydiacetylene fibre–epoxy resin matrix (for which $E_f/E_m = 16$) [19] are also shown. Compared with the previous analytical solution, the present analytical solution agrees better with both the numerical and the experimental results. It is noted that the predicted curve should intercept the x axis at a value greater than unity (i.e. $E_f/E_m > 1$ when $l_c/a = 0$) in Fig. 5. This is because the axial stress in a discontinuous fibre is always equal to that of an infinitely long fibre (and the applied stress) when $E_f = E_m$ (i.e. $\sigma_f = \sigma_0$ when $E_f = E_m$). It is not clear why the l_c/a against E_f/E_m curve passes through the original in the finite difference results.

4.4. Effects of the Young's modulus ratio

The normalized axial stress, the normalized interfacial shear stress, and the normalized axial strain as functions of the normalized axial position are shown in Fig. 6a, b and c, respectively, at different E_f/E_m ratios. Stress transfer from the matrix to the fibre increases

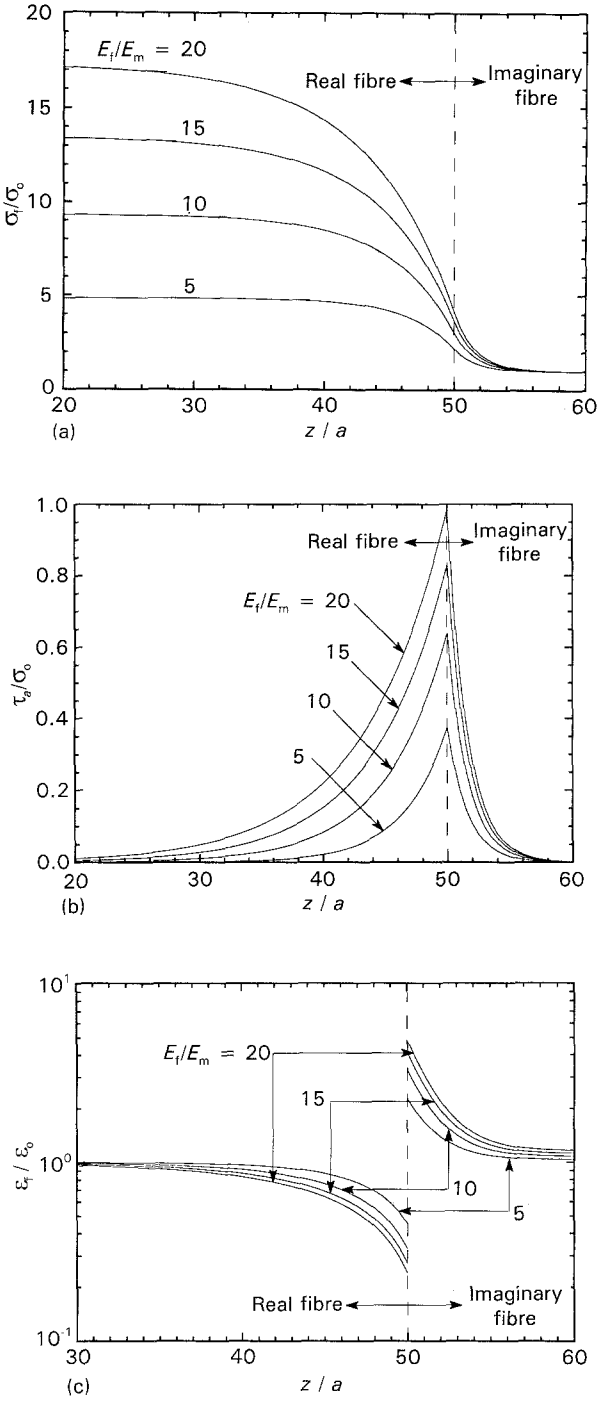

Figure 6 (a) Normalized axial stress, σ_f/σ_0 (and σ_f'/σ_0), (b) the normalized interfacial shear stress, τ_a/σ_0 (and τ_a'/σ_0), and (c) the normalized axial strain, $\varepsilon_f/\varepsilon_0$ (and $\varepsilon_f'/\varepsilon_0$), as a function of normalized position, z/a, at different E_f/E_m ratios.

with an increase in the ratio E_f/E_m (Fig. 6a). With the interfacial shear stress proportional to the stress gradient in the fibre, the interfacial shear stress increases with an increase in E_f/E_m (Fig. 6b). The axial strain is normalized by the equilibrium axial strain in the composite, ε_0, in Fig. 6c. The trends predicted in Fig. 6b and c agree with those predicted from the finite difference results (see Figs 3 and 4 in Termonia [17]).

5. Conclusions

The elastic stress transfer from the matrix to the embedded fibre in fibre-reinforced composites has been

analysed by using the shear lag model. Solutions for stress transfer are subjected to the boundary condition at the fibre ends. When the fibre ends are debonded from the matrix, they are stress-free and the boundary condition in solving the stress transfer problem is trivial. When the fibre ends are bonded to the matrix, stress transfer also occurs at the ends, such that the stress at the bonded ends is finite. However, there is ambiguity in defining this finite stress. An approximation has been made previously to obtain analytical solutions for the bonded-ends case.

The previous analytical solution for the bonded-ends case [12] is modified in the present study. This is achieved by adding imaginary fibres to the model and satisfying the continuity condition at the boundary between the imaginary and the real fibres. Compared to the previous analytical solution [12], the present analytical solution bears more physical meaning and agrees better with the numerical [17] and the experimental results [19]. The effects on stress transfer of the distance between the fibre end and the loading surface, the aspect ratio of the fibre, and the Young's modulus ratio of fibre to matrix are also studied.

Acknowledgements

The author thanks Drs P. F. Becher, H. T. Lin and E. Lara-Curzio for reviewing the manuscript. The research was jointly sponsored by the US Department of Energy, Division of Materials Sciences, and the Assistant Secretary for Conservation and Renewable Energy, Office of Industrial Technologies, Industrial Energy Efficiency Division, under contract DE-AC05-84OR21400 with Martin Marietta Energy Systems, Inc.

References

1. A. G. EVANS and R. M. McMEEKING, *Acta Metall.* **34** (1986) 2435.
2. P. F. BECHER, C. H. HSUEH, P. ANGELINI and T. N. TIEGS, *J. Am. Ceram. Soc.* **71** (1988) 1050.
3. H. L. COX, *Br. J. Appl. Phy.* **3** (1952) 72.
4. A. TAKAKU and R. G. C. ARRIDGE, *J. Phys. D: Appl. Phys.* **6** (1973) 2038.
5. P. LAWRENCE, *J. Mater. Sci.* **7** (1972) 1.
6. M. R. PIGGOTT, "Load Bearing Fibre Composites" (Pergamon, Elmsford, New York, 1980) p. 62.
7. B. BUDIANSKY, J. W. HUTCHINSON and A. G. EVANS, *J. Mech. Phys. Solids* **34** (1986) 167.
8. H. STANG and S. P. SHAH, *J. Mater. Sci* **21** (1986) 953.
9. C. H. HSUEH, *J. Mater. Sci. Lett.* **7** (1988) 497.
10. D. K. SHETTY, *J. Am. Ceram. Soc.* **71** (1988) C107.
11. Y. C. GAO, Y. W. MAI and B. COTTERELL, *J. Appl. Math. and Phys. (ZAMP)* **39** (1988) 550.
12. C. H. HSUEH, *J. Mater. Sci.* **24** (1989) 4475.
13. R. J. KERANS and T. A. PARTHASARATHY, *J. Am. Ceram. Soc.* **74** (1991) 1585.
14. C. H. HSUEH, *Mater. Sci Eng.* **A154** (1992) 125.
15. G. E. SMITH and A. J. SPENCER, *J. Mech, Phys. Solids* **18** (1970) 81.
16. A. S. CARRARA and F. J. McGARRY, *J. Compos. Mater.* **2** (1968) 222.
17. Y. TERMONIA, *ibid.* **22** (1987) 504.
18. B. F. BLUMENTRITT, B. T. Vu and S. L. COOPER, *Polym. Eng. Sci.* **14** (1974) 633.
19. C. GALIOTIS, R. J. YOUNG, P. H. J. YEUNG and D. N. BATCHELDER, *J. Mater. Sci.* **19** (1984) 3640.

Received 6 September 1993
and accepted 13 June 1994